A Recreation Mathematical Model of the Lateral Pyloric Cell of the Stomatogastric Ganglion

Tyler Burleyson

Case Western Reserve University

A Recreation Mathematical Model of the Lateral Pyloric Cell of the Stomatogastric Ganglion 1

Background

The paper "Mathematical Model of an Identified Stomatogastric Ganglion Neuron", by Frank Buchholtz, Jorge Golowasch, Irving Epstein, and Eve Marder is the second in a three-paper series describing the lateral pyloric (LP) cell in the stomatogastric ganglion (STG) of the crab *Cancer Borealis*. (Golowasch & Marder, 1992; Buchholtz et al, 1992; Golowasch et. al, 1992). In particular, this paper models the six voltage-dependent currents, a Ca^{2+} buffering system, and the membrane capacitance (all found experimentally) and creates a single-compartment, isopotential model of the entire cell.

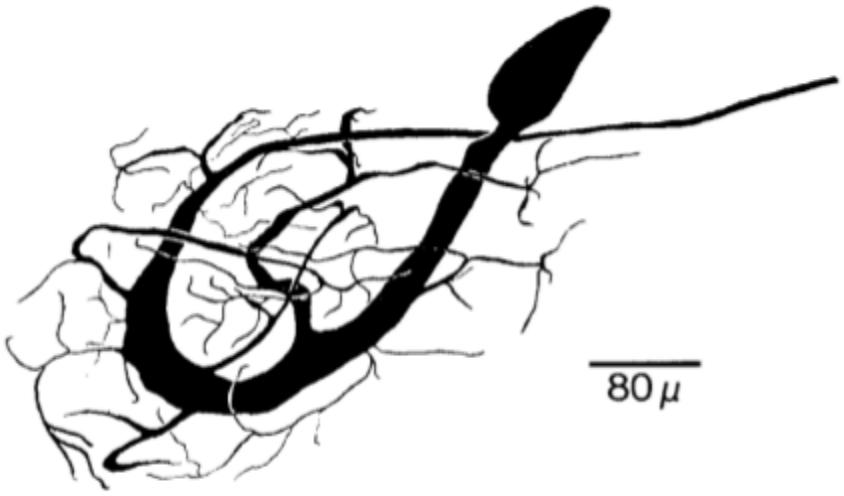

Figure 1. A drawing of the LP cell in the stomatogastric ganglion of the crab *cancer borealis*. Adapted from "Ionic Currents of the Lateral Pyloric Neuron of the Stomatogastric Ganglion of the Crab," by Jorge Golowasch and Eve Marder. February 1992, *Journal of Neurophysiology*, Vol. 67 No. 2

The voltage-dependent currents are as follows: delayed rectifier-like; Ca^{2+}-activated outward; transient A-like; Ca^{2+} inward; inwardly rectifying; and fast tetrodotoxin (TTX)-sensitive Na^{+}, as well as a voltage-independent leak current. The currents are called 'voltage-dependent' because their amplitudes depend on the difference in potential across the cell membrane; the Ca^{2+}-activated outward current depends on the concentration of calcium ions as well. Most of the currents affect potassium ions, with the exceptions of the Ca^{2+} inward and fast Na^{+} currents, which affect their titular ions.

The currents are summed and subtracted from an external current to simulate current-clamp biological experiments, and voltage clamp experiments can be simulated by setting voltage to a value manually.

The advantages of studying a mathematical model of the neuron are numerous. Firstly, many methods of studying currents require voltage-clamp experiments. Researchers using this method assume that synaptic conductances are voltage-independent, an assertion incorrect for a variety of reasons discussed by Anton Chizhov and Dmitry Amahkin in their paper "Method of experimental synaptic conductance estimation: Limitations of the basic approach and extension to voltage-dependent conductances" (Chizhov & Amahkin, 2017). A mathematical model provides a way to study the cell without necessarily relying on these techniques. There are also conveniences that come with the model, such as allowing researchers to increase or decrease conductance of individual currents, as well as examine currents independently of each other. On occasion (and as is the case of the fast Na^+ current) this includes currents which can't be directly measured in experimental settings. The model can then be compared against biological data obtained in voltage-clamp and other experiments to corroborate accuracy.

The paper aims to describe the contribution of each current to the overall dynamic properties of the cell. Similarly, we hypothesize that the identified currents can approximate biological data when given a similar stimulus, and then be considered individually to further explain the effect of each current on overall potential despite the relative simplicity of the model.

Significance

The paper is well-cited, both for its biological data (Fox, 2017; DeMaegd, 2018, pg. 16), it's deterministic qualities (Herrera-Valdez, 2012), and its identified currents (Daur et. al, 2012).

The stomatogastric ganglion is an important cell in the crab, controlling several muscles in the foregut. The LP neuron itself directs multiple connections through the neuropil of the STG, in part affecting motor patterns (Golowasch & Marder, 1992). As stated above, the mathematical model has several advantages over direct biological study in furthering understanding of each current. While this model is relatively simple, its power in recreating biological data accurately lends it value in closer study.

Description of Results and Extension

This model proved particularly recalcitrant in my partner and I's attempts to recreate it. Numerous discrepancies appeared throughout the process, all of which will be further explored below. Many figures depicting individual currents and their steady-state equations were replicated well using the paper's given parameters and methods of finding initial values. However, more complex currents proved to be too sensitive to the apparent errors in the paper, and full cell replication was not possible at first.

As an extension then, we built Manipulate figures using the mathematical computation programming language Mathematica's Manipulate function to attempt to find parameter values which would coax accurate behavior out of the model. The original authors note that they adjusted values in the fast Na^+ current and the membrane capacitance, so naturally we began there, before using our understanding of the interrelated dynamics of the currents to further manipulate the model.

Model Description

Parameters

Each of the currents present in the model is defined by a similar equation, as will be described in the next section. Thus there are general parameters with specific values for each, as well as some extra parameters specific to the more complicated currents. All parameters are experimentally derived, with several important exceptions explained below.

Table 1: Parameters

TABLE 1. *Parameters used in the model*

Conductance	Maximum Conductance $\bar{g}_j$, μS	Reversal Potential E_j, mV	Rate Constant, s^{-1}	Half-Maximum Potential, mV	Step Width, mV	Other Parameters
Delayed rectifier, i_d	$\bar{g}_d = 0.35$	$E_K = -80$	$c_n = 180$	$V_n = -25$ $V_{hn} = 10$	$s_n = -17$ $s_{hn} = -22$	
Calcium-activated outward current, $i_{o(Ca)}$	$\bar{g}_{o(Ca)} = 3.2$	$E_K = -80$	$k_{oa} = 600$ $k_{ob} = 35$ $k_{Ca} = 360$	$V_{ao1} = 0$ $V_{ao2} = -16$	$s_{ao1} = -23$ $s_{ao2} = -5$	$f = 0.6$ mV/μM $c_1 = 2.5$ μM $c_2 = 0.7$ μM $c_3 = 0.6$ μM $[Ca^o] = 0.05$ μM $c_{iCa} = 300$ μM/nC
A-current, i_A	$\bar{g}_A = 2.2$	$E_K = -80$	$k_A = 140$ $k_{A1} = 50$ $c_{A2} = 3.6$	$V_A = -12$ $V_B = -62$ $V_{A2} = -40$ $V_X = 7$	$s_A = -26$ $s_B = 6$ $s_{A2} = -12$ $s_X = -15$	
Ca^{2+} current, i_{Ca}	$\bar{g}_{Ca1} = 0.21$ $\bar{g}_{Ca2} = 0.047$	E_{Ca}*	$k_{aCa1} = 50$ $k_{bCa1} = 16$ $k_{aCa2} = 10$	$V_{aCa1} = -11$ $V_{bCa1} = -50$ $V_{aCa2} = 22$	$s_{aCa1} = -7$ $s_{bCa1} = 8$ $s_{aCa2} = -7$	
Inward rectifier, i_h	$\bar{g}_h = 0.037$	$E_h = -10$	$c_r = 0.33$	$V_r = -70$ $V_{hr} = -110$	$s_r = 7$ $s_{hr} = -13$	
Fast Na^+ current, i_{Na}	$\bar{g}_{Na} = 2{,}300$	$E_{Na} = 50$	$k_m = 10{,}000$ $k_h = 500$	$V_{am} = -6$ $V_{bm} = -34$ $V_{ah} = -39$ $V_{bh} = -40$	$s_{am} = -20$ $s_{bm} = -13$ $s_{ah} = -8$ $s_{bh} = -5$	$c_{am} = 0.11$ mV^{-1} $c_{bm} = 15$ $c_{ah} = 0.08$
Leak current, i_l	$\bar{g}_l = 0.1$	$E_l = -50$				$c_m = 1.7$ nF

* $E_{Ca} = [R \cdot T/z \cdot F] \cdot \ln(13{,}000/[Ca^{2+}]_{in}) + 1{,}000$, and T was 283°K (10°C).

Table 1. *Parameters used in the model*. (Buchholtz et. al., 1992, p. 333)

The maximum conductance, $\overline{g}$, represents the highest possible flow of the specific current. Varying the maximum conductance will directly adjust the magnitude of the effect of the current on cell behavior, which we take advantage of in our extension.

The reversal potential (or Nernst) potential, E_j, is the charge at which charged particles are equally repelled from and attracted to moving through the channel. It is calculated by

$$E_{ion} = RT/zF \ln([C]_{out}/[C]_{in}) \quad (1)$$

An equation from Chapter 7 of our course textbook (Hillel, eq. 7.3.4). In the model, E_j is a constant for all flows except for i_{Ca}. Because this relies on the concentration of calcium, and also affects said concentration, it is defined by the following equation provided in the paper:

$$E_{Ca}=(R(T/z)F)\ln(13{,}000/[Ca^{2+}]_{in})*1000 \quad (2)$$

Assuming T=298K.

The rate constant appears in certain relaxation equations, which describe the impact of voltage on activation and the rate at which the activation decreases. The rate constant scales these values so that relaxation will correspond to experimental data.

The half-maximal potential, V_a, represents the potential where the voltage-dependent steady state equation is equal to ½. It causes the steady state equations to equal one at that voltage.

The step width, s_a, according to the paper, is "the step width of the curve (i.e., the range of potentials centered at V_a over which $a_\infty(V)$ [the voltage-dependence steady state equation] varies from ~0 to ~1)" (Buchholtz et. al., 1992, p. 333). The s_a values can be positive or negative, indicating functions that increase with V or decrease with V, respectively. While typically negative values indicate activation (and vice versa), in the case of the inwardly-rectifying i_h, this relationship is inverted.

The Ca^{2+}-activated outward current has several specific parameters. $[Ca^{2+}]^0$ denotes initial calcium concentration in the cell. Several other constants represent calcium concentrations obtained from previous literature. Finally, c_{iCa} provides a ratio between calcium concentration and the cell's volume. It is calculated by

$$C_{iCa}=1/(z*F*Vol) \quad (3)$$

Where z is the valence of Ca^{2+}, F is the Faraday constant, and Vol is volume. In order to match the model to experimental data, the authors used a c_{iCa} value much larger than determined by the equation, implying that the effective volume is much smaller than that of the cell. The authors theorize that this "probably corresponds to the immediate vicinity of the inner cytoplasmic membrane" (Buchholtz et. al., 1992, p. 335).

State Variables

In addition to the voltage over the cell and the calcium concentration, each current has varying individual state variables corresponding to activations and inactivations. In total, there are seven activations, six inactivations, membrane potential, and calcium concentration, for a total of 14 state variables. In addition, each of the activations and inactivations have varying numbers of steady state functions describing their voltage-dependencies. Each activation and inactivation is a scalar describing the level of activity of the current. For example, a low activation and a high inactivation will cause muted activity: and vice versa. Biologically, they represent the opening and closing of gates in the membrane, which enable ion flow and voltage across the membrane. The calcium concentration affects the activity of the outward calcium current, and is affected itself by the inward calcium concentration. Finally, the membrane potential is calculated by the following equation:

$$c_m * dV/dt = i_{ext} - \sum_j i_j \quad (4)$$

Where c_m represents the capacitance of the membrane, dV/dt is the rate of change of voltage across the membrane, i_{ext} is an externally applied current in current clamp experiments (e.g., experimental setups in which the current is held at a steady value).

Currents

The following table provides descriptions and the equation of each current. Activations will be highlighted in green, and inactivations in red. Note also that V represents the voltage across the cell throughout. The term $(V - E_j)$ is referred to as the driving force, as it is what directly causes change in membrane potential.

Table 2: Current Descriptions

Current	*Description*	*Equation*
Delayed Rectifier	An outward current with a long voltage-dependent delay and no inactivation. It acts in the cell as a rectifier acts in a circuit. There is a single activation present.	$i_d = g_d * n^4 * (V - E_k)$
Ca^{2+} outward-activated	This current is relatively complex. It relies on calcium concentration for its activation and inactivation factors, which in turn is affected by the inward calcium current. There is an activation and an inactivation present.	$i_{0Ca} = \overline{g}_{0(Ca)} * a_0 * b_0 * (V - E_k)$
Transient A-like	The current has two inactivation factors, and a weighting factor to determine which controls it; the slower term is favored at low voltages, and the faster term at depolarized voltages. There is a single activation and two inactivations scaled by a weighting factor, x(V), which determines which inactivation dominates the term.	$i_A = \overline{g}_A * a_A^3 * \{x(V)*b_{A1} + [1 - x(V)] * b_{A2}\} * (V - E_k)$
Ca^{2+}	There are two components displaced in voltage from one another controlling the current. The first has an inactivation factor, and the second does not. They are summed to determine the overall impact. This affects the amount of Calcium in the cell. There are two activations and an inactivation present.	$i_{Ca} = (\overline{g}_{Ca1} * a_{Ca1} * b_{Ca1} + \overline{g}_{Ca2} * a_{Ca2}) * (V-E_{Ca})$

Inwardly Rectifying, or Hyperpolarization Activated	This slow current is activated at voltages more hyperpolarized than the resting potential. There is no inactivation observed, or included in the model. Instead, it's single relaxation rate cause it to diminish as the cell grows less polarized.	$I_h = \overline{g}_h * r * (V - E_h)$
Fast Na^+	The current is generated far from the cell body, and thus not measurable in biological experiments. The activation is much faster than any other current, and in the model is instantaneous. The parameters were set so as to observe firing action potentials. The voltage dependencies are in Hodgkin-Huxley form. There is a single activation and inactivation present.	$i_{Na} = \overline{g}_{Na} * m^3 * h * (V - E_{Na})$
Leak	The linear component of the steady-state current-voltage (I-V) curve. This lacks an activation or inactivation, as it is linear. Maximum capacitance was measured by the input conductance of the LP neurons in the region of the I-V curve with lowest conductance. There are no activation or inactivations, as this is voltage-independent.	$i_l = \overline{g}_l * (V - E_l)$

Each activation and inactivation has a voltage dependence steady-state equation, and some have additional equations of the same form describing the voltage-dependent relaxation of the current. The general form for these equations is

$$a_\infty(V) = 1/\{1+Exp[(V-V_a)/s_a\} \quad (5)$$

Since each of these equations is similar beyond changing parameters and additional, identical terms, it is beyond the scope of this description to list all explicitly.

Model Assumptions

The most significant assumption made by the model is the choice of a single-compartmental, isopotential model. It is known that the LP neuron has multiple compartments, and more complex models consider it thusly. In fact, Buchholtz indicates unpublished findings of a dual-compartment model showing "improved robustness and attenuated action potentials" (Buchholtz et. al., 1992, p. 338). Furthermore, the authors note that their model "is more properly thought of as a model of the cell at the action-potential initiation zone" (Buchholtz et. al., 1992, p. 338).

Further assumptions change parameter values to better align the model with the experimental data. The most significant of these is the change to c_m, the membrane capacitance. The model value is about 10 times lower than that measured, likely corresponding with the assumption that this model better describes the initiation zone than the cell as a whole. Notable as well is that the values of the Na^+ current could not be measured experimentally, and so are based on Hodgkin-Huxley equations. Parameters were chosen specifically to obtain action potentials after integration, an important note since this current plays a dominant role in action potential generation. These two and other conductance values are varied to manipulate cell behavior in our extension.

Simulation

The paper constructs time plots of several currents depicting amplitude over time, as well as plots of steady state values normalized and compared. In order to do this, a Mathematica notebook is set up as follows.

Each current begins in its own notebook. It has a cell initializing its parameters, it's voltage dependence equations, and then the NDSolve function, a numerical differential equation solver, is used to calculate initial activation. This is done by setting voltage to the holding voltage, V_h identified in the paper (-40 mV). The equation is allowed to reach a steady-state value, which is then used as the initial activation. This is a key step in obtaining data relevant to experimental data, since experimental data depends on the steady state the current existed in prior to manipulation.

Since the current depends on activations and inactivations, these are placed into a single NDSolve function within Mathematica, which can evaluate them simultaneously over the same period. We can then plot this equation to obtain graphs like figure 1A above. Multiple lines appear when the voltage is given multiple initial values, representing "pulses" of that voltage being passed over the membrane. These can be graphed over each other.

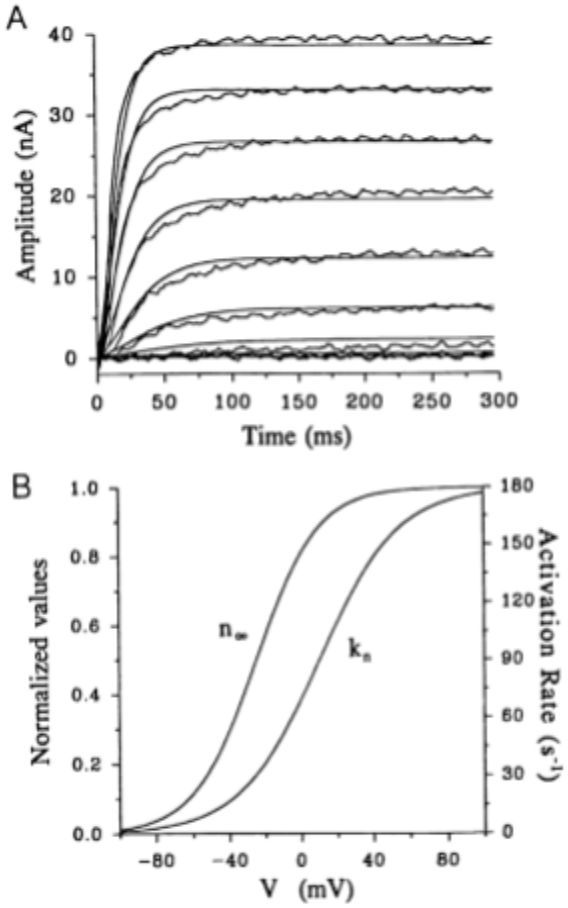

Figure 2. Two graphs depicting A. amplitudes of the delayed rectifier over time, and B. normalized activation rates of the steady state activation and relaxation of the delayed rectifier current. (Buchholtz et. al., 1992, p. 333)

The relaxations and voltage dependencies are graphed by simply plotting their equations over a set range of voltages. The voltage dependence is designed to be between 0 and 1, while relaxation can have a wider range of values. Relaxation is normalized by dividing by the value of the relaxation at the minimum voltage graphed. These can then be overlayed to obtain graphs like figure 2B.

Our extension is accomplished by a Manipulate function. We can insert the full cell model into a Manipulate and vary the maximum conductances of each current, allowing us to 'turn off' currents and observe the exact effects they each have on model performance. We will first break down the model to three currents, then add the rest as we look for more and more accurate behavior. The end goal of this extension is largely to more exactly understand the dynamic properties of each current within the cell.

Results

Figure 3

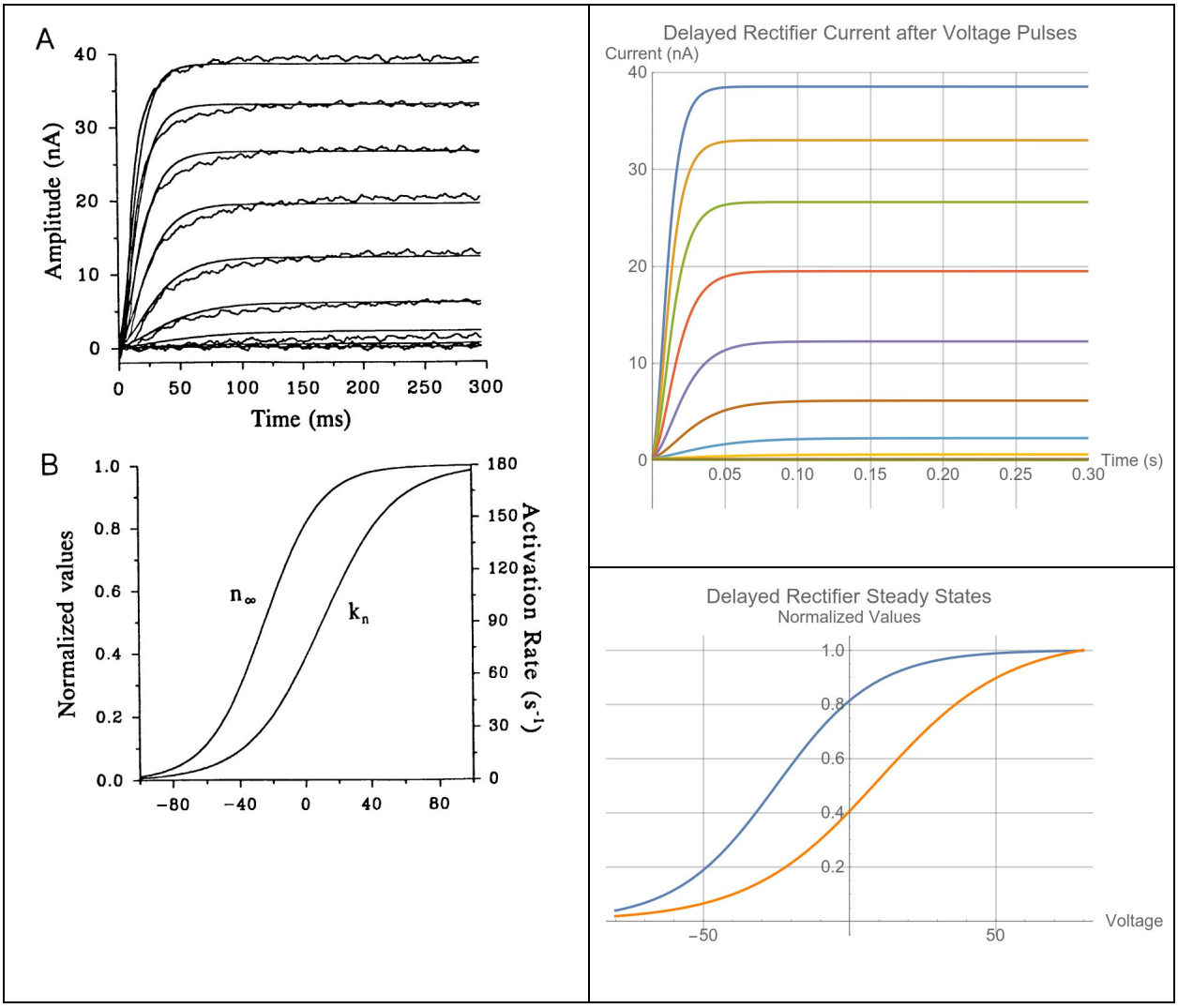

Figure 1, Buccholtz et. al., (1992) *(left)*, and Figure 3A *(top right)* & B *(bottom right)* my result done in Mathematica (see attached notebook). In 3A of both original and my result, voltages pulses of -50, … 30 mV in steps of 10 mV are arranged top to bottom. The paper's graph includes noisy experimental data overlaid with model results. In my 3B graph, the blue curve represents n_∞ and the orange curve represents k_n.

Figure 3 describes the delayed rectifier current identified in the original paper, *Ionic currents of the Lateral Pyloric Neuron of the Stomatogastric Ganglion of the Crab* by Golowasch et. al. A delayed rectifier current is a common feature in neurons, where it's voltage dependence and delay in onset (not showing in experimental data until voltages of -40mV or higher are clamped) are easily spotted (1992a). In these aspects, our results mirror perfectly those found in the paper. This is an exemplar of the capacity of modeling to isolate current; the delayed rectifier is easily identified experimentally, and easily replicable on its own. This replication can then be inserted into the full model, and affect the model behavior just as the real current affects the cell. This lends a great deal of credence to our hypothesis.

Figure 4

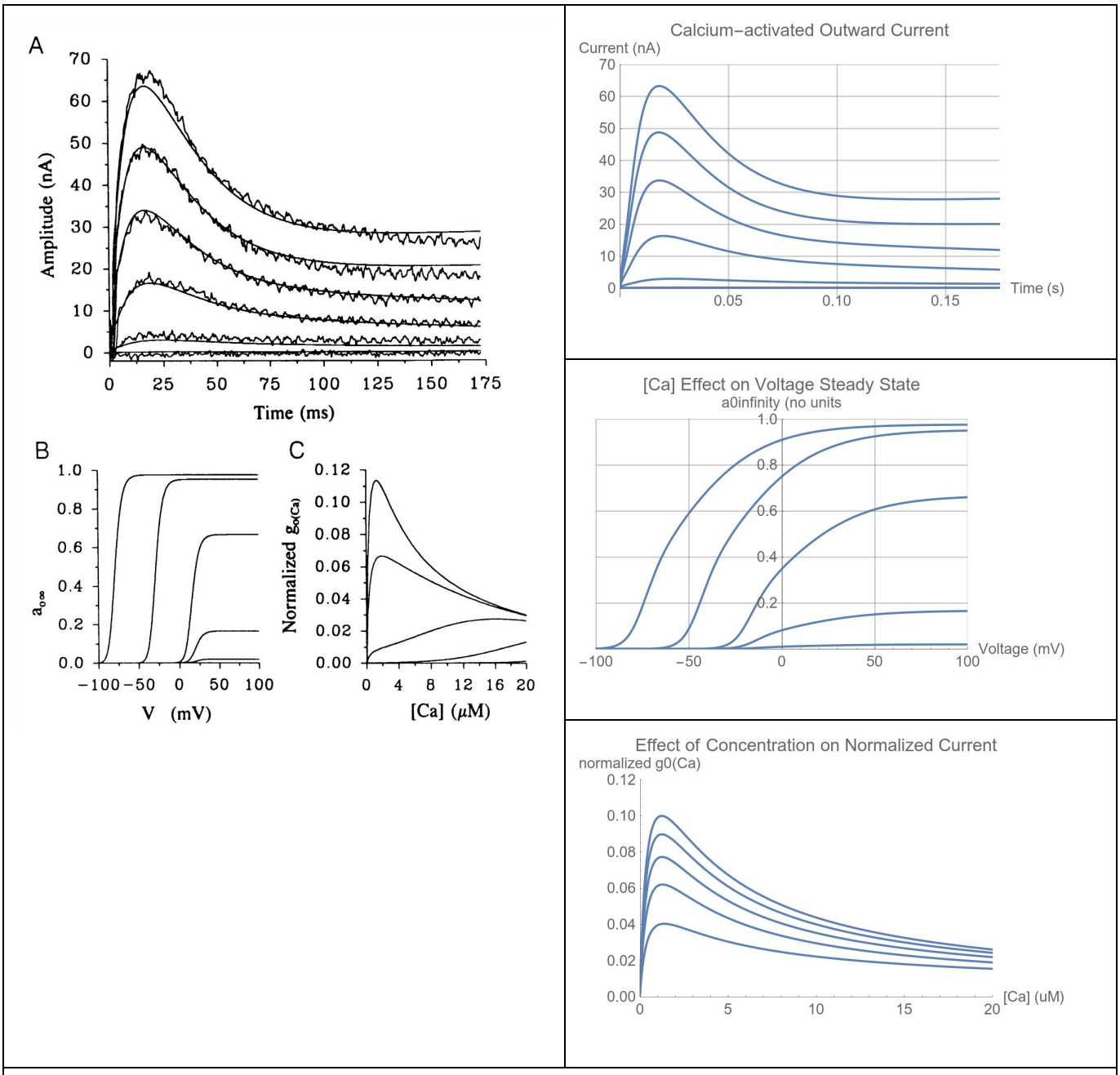

Figure 2, Buchholtz et. al., (1992) *(left)* Figure 4A *(top right),* B *(middle right)*, C *(bottom right)* my results done in Mathematica. A: Voltage pulses from -30, … 20 mV in steps of 10 mV were applied. Noisy experimental data is overlaid by model output. B: Voltage dependency was calculated at calcium concentrations of 100, 50, 5, 0.5, and 0.05. C: Voltage is held constant at 30, … -10 mV in steps of 10mV.

The calcium-activated current, calcium current, and calcium buffer system are by far the most interrelated of the elements of the model. Calcium concentration is defined by its own state variable and equation which relies upon the inward calcium current. The calcium-activated current thus depends on both for its Nernst potential.

Interestingly, the graph of the outward current (which relies upon all elements of the calcium system) is identical between our results and those of the author, while the steady state graphs and normalized current as a result of calcium concentration differ greatly. Our graph features a longer initial lag and a much shallower slope compared to those found in the paper. After a thorough examination of parameters and the voltage-dependent equations, we were unable to find discrepancies between our work and that discussed by the authors. By varying the step size of the first activation steady state equation, we are able to rectify the differences noted above, but the altered parameter greatly inflates the value of the current in 4A. Frustratingly (or perhaps amusingly), that reinforces our original observation that we were able to obtain the highest level result, but unable to replicate a much simpler dependency for said result. As noted in the paper, the literature suggests the steepness and shift of the curves is reflected in the literature. We replicate the shifts, but do not see nearly the expected steepness (Buchholtz 334).

Figure 4C shares a similar story. Our results show identical behavior at varying levels of intensity, while the paper shows qualitative changes in behavior at positive, 0-valued, and negative voltages.

Overall, the complications inherent in the calcium system prove difficult or impossible to isolate as we were able to the delayed rectifier. This wrinkle in the model suggests that our

original hypothesis may be true only in a limited scope: for simpler, singular currents like the delayed rectifier.

Figure 5

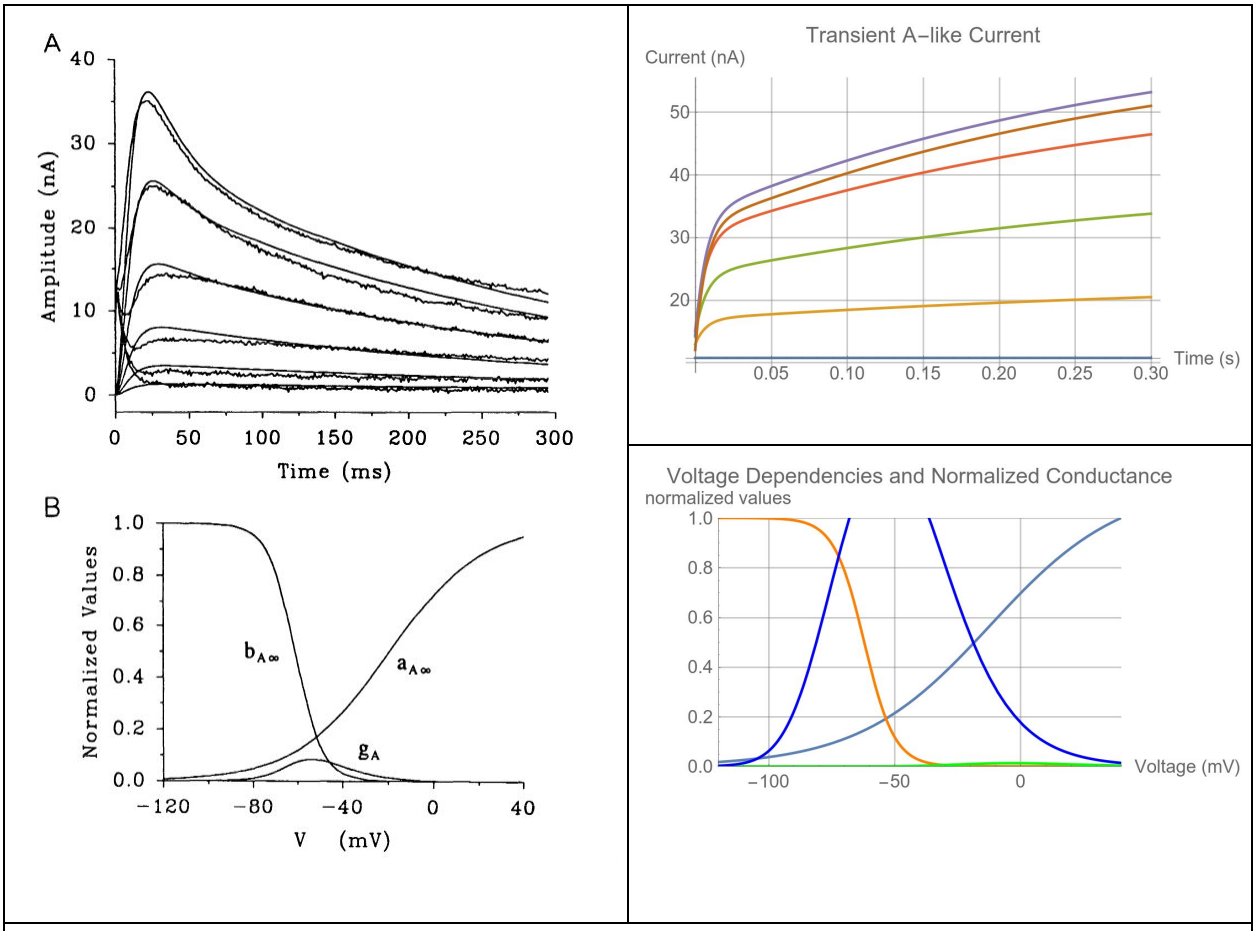

Figure 3, Buchholtz et. al. (1992) *(left)*, Figure 5A *(top right)* & B *(bottom right)* from my results. A: a plot of the A-like potassium current against time. From bottom to top within the graph, voltage pulses of -40, … 10 mV in steps of 10 mV are plotted. Noisy experimental data is overlaid with model results in the paper. B: Voltage dependency steady states are graphed, along with normalized conductance. The orange line indicates the first inactivation, the light blue line activation, and the green and dark blue lines attempts at the normalized conductance curve.

The transient A-like current is a fast potassium current found in the cell. It is notable for its unconventional inactivation, in which two separate processes are weighted against each other,

allowing for differing behaviors at depolarized and hyperpolarized voltages. This is shown well by the paper's graph, in which positive and negative voltage pulses have qualitatively different results as would be expected. Unfortunately, these results proved irreproducible from the paper's equations and parameters. We attempted to lower the power of the activation from three to one[1]. This led to an increase in the magnitude of our graph (note the different y-axes in order to show the data more fully) -- an understandable change since the scalar activation value always falls between zero and one.

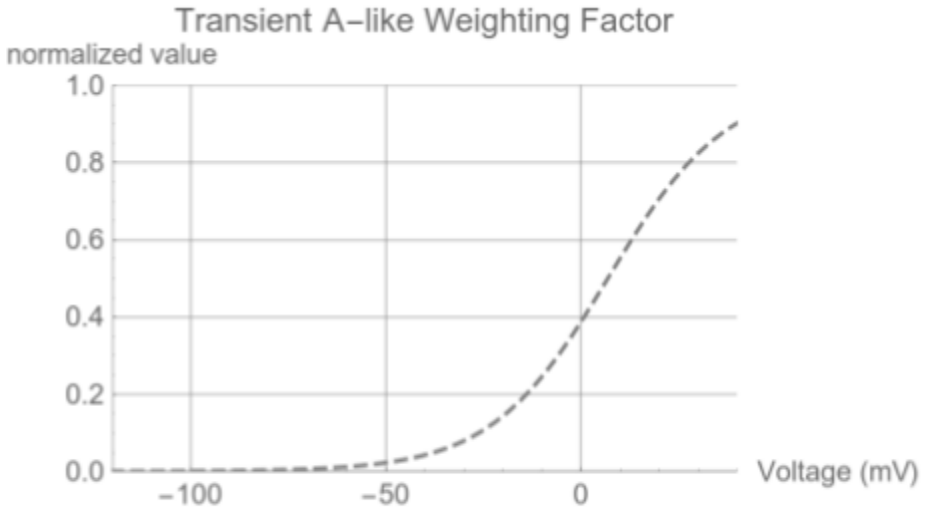

Figure 6. This is not a result shown explicitly in the paper, but rather one generated during our research to explain the function of the weighting factor. Since the second inactivation is multipled by 1-x(V), where x(V) is the weighting factor, at positive voltages it is suppressed, but at negative voltages it is allowed to dominate.

Upon graphing, it was revealed that the second inactivation process behaved more similarly to an activation than an inactivation; namely, it was high at hyperpolarized values and low at depolarized values. That reversal is found experimentally as well (Golowasch et. al., 1992, pg. 325). This behavior is suppressed by the weighting factor as described above in the caption of figure 6, allowing the first, more traditional inactivation, to dominate. This allows for the behavior seen in the Buchholtz's figure 2A, where negative voltage pulses generate large spikes and positive pulses cause little perturbation (Buchholtz et. al., 1992, p. 334). This can be

[1] Thanks goes to Dr. Hilel Chiel for the suggested course of action.

likened to the relevant gates remaining closed under similar experimental conditions in the neuron. The components are broken down nicely here to explain the biological and mathematical significance of the current and its factors, implying our hypothesis.

Figure 7

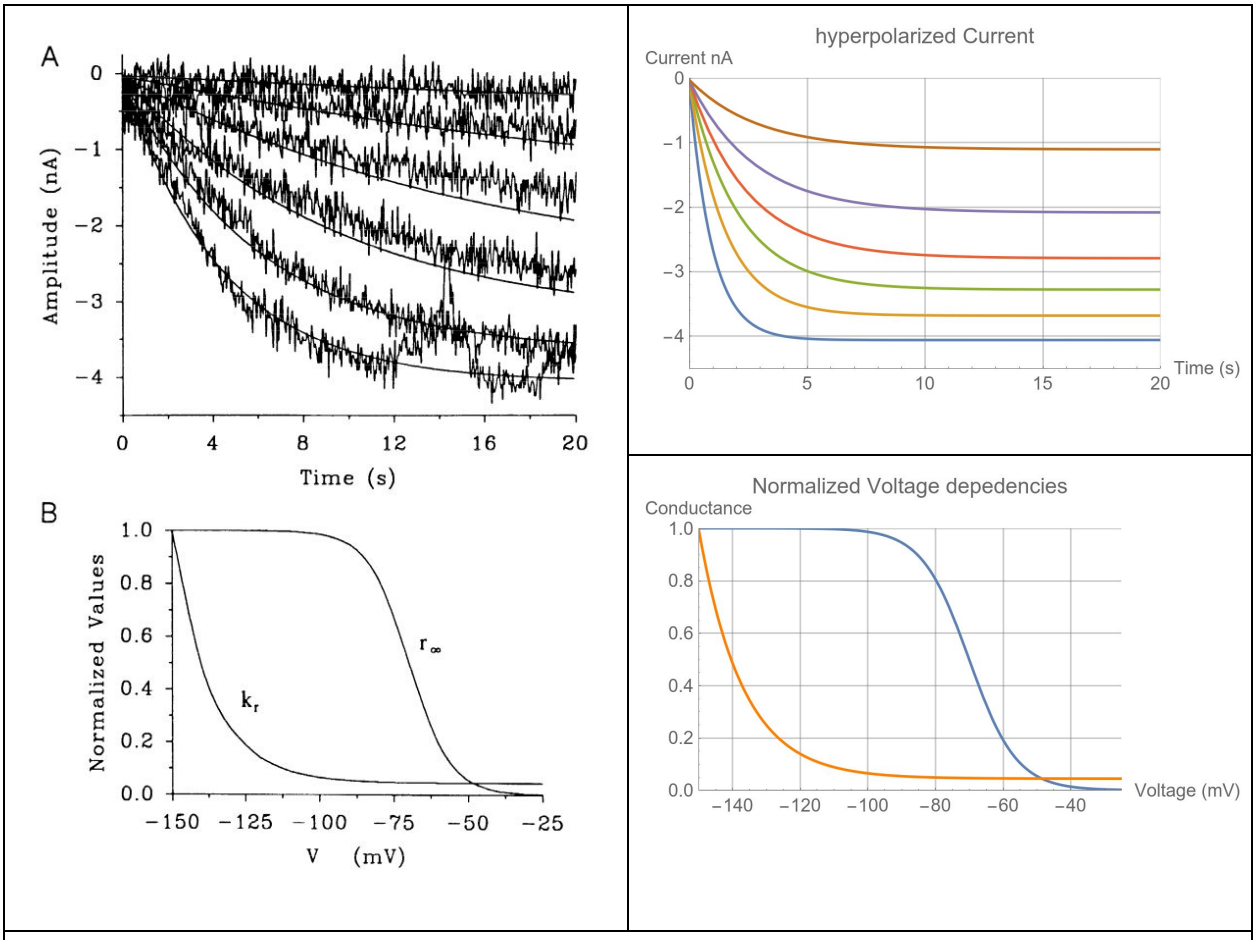

Figure 4, Buchholtz et. al., (1992) *(left)* and Figure 7A *(top right)* & B *(bottom right)* from my results done in Mathematica. A: voltage was stepped to -120, … -70 mV in steps of 10 mV from top to bottom. On the left, noisy experimental data is overlaid. B: normalized steady state values. On my graph, the orange curve represents relaxation rate k_r and the blue curve represents activation r_∞.

The slow, inward i_h current activates at voltages more hyperpolarized than the resting potential, -45 mV. In figure 7B this becomes apparent by the low relaxation value at that potential. Note the length of the axes compared to the other figures: the current is orders of magnitude smaller and slower. This reflects the rather minor effect that i_h has on the overall function of the cell.

Compared to the paper's graph, our results in figure 7A appear to reach maximal amplitude earlier, and show more strongly asymptotic behavior. Minimal explanation of the current is given in the original paper, making diagnosis of our issues particularly difficult. Ultimately we would not expect this slight discrepancy to have a large effect on the cell as a whole due to its slight magnitude and the common end behavior.

Figure 8

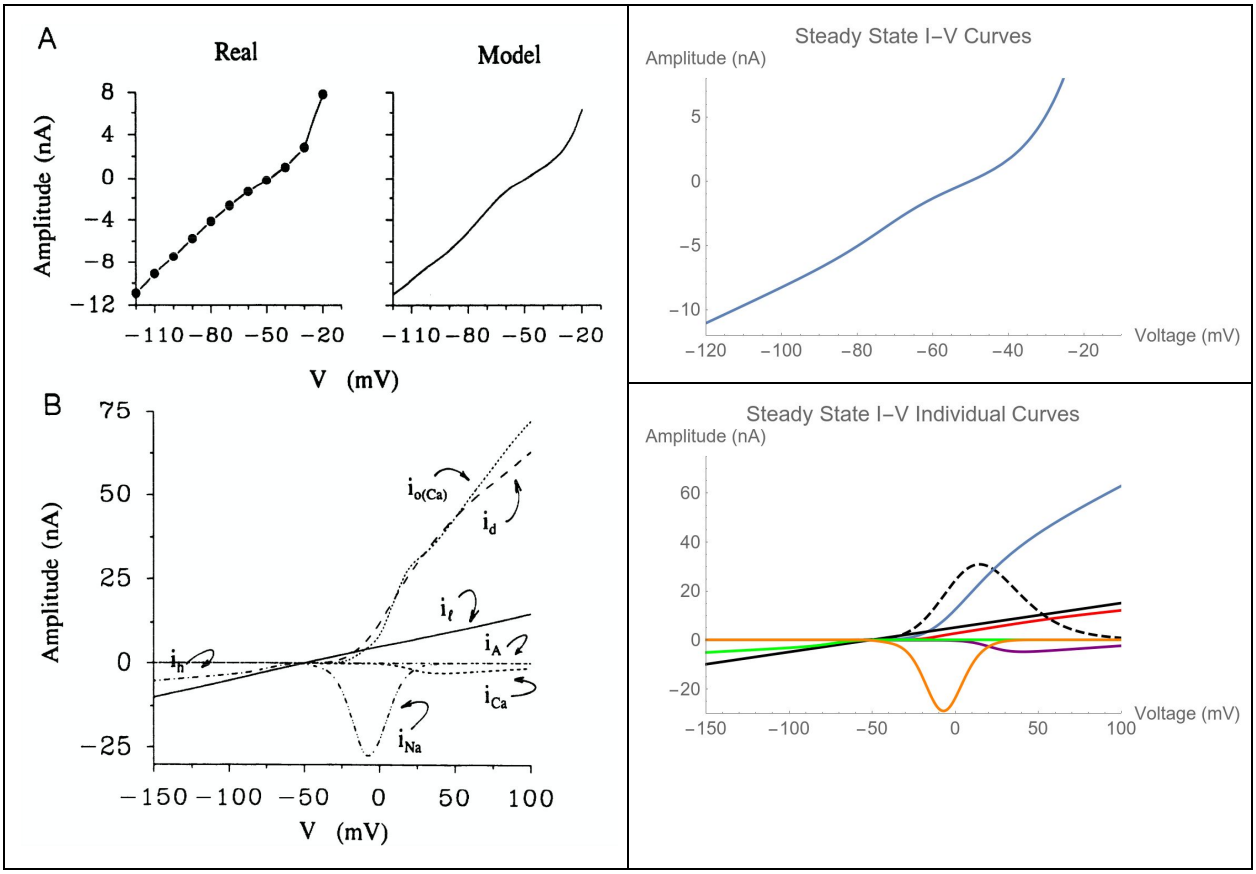

Figure 6, Buchholtz et. al., (1992) *(left)* and Figure 8A *(top right)* & B *(bottom right)* from my results done in Mathematica. A: Steady state I-V curves for the model and experimental data. The sodium current is removed in all. B: Individual current I-V curves. In my graph, the delayed rectifier is black, the sodium is orange, the hyperpolarized activated is green, the transient A-like is black and dashed, the leak is a black straight line, and the outward calcium is red.

The graphs show that experimental steady-state properties are matched rather well. The zero current point, where all currents have zero amplitude, is at about -45 to -50 mV, as was found in experiments. More depolarized voltages saw stronger steady state behaviour out of the currents as well.

Extension Results

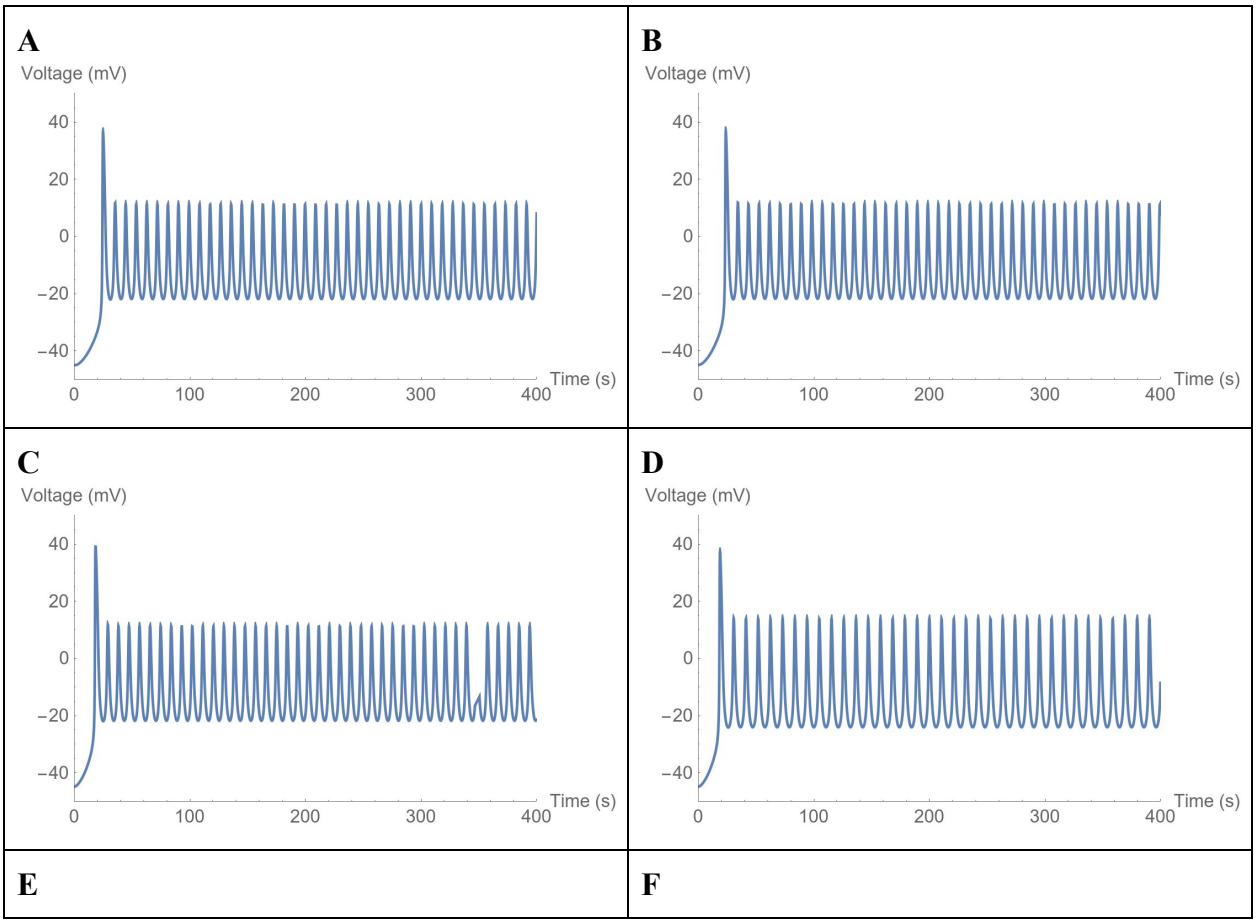

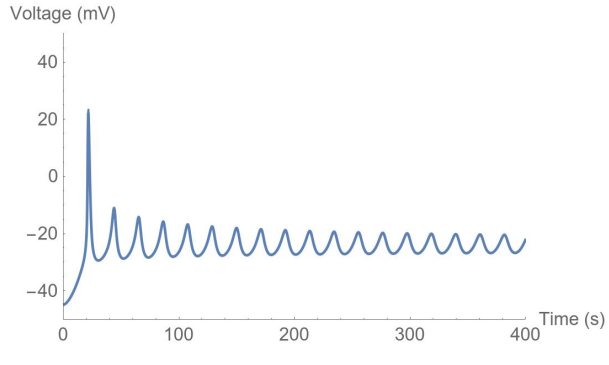

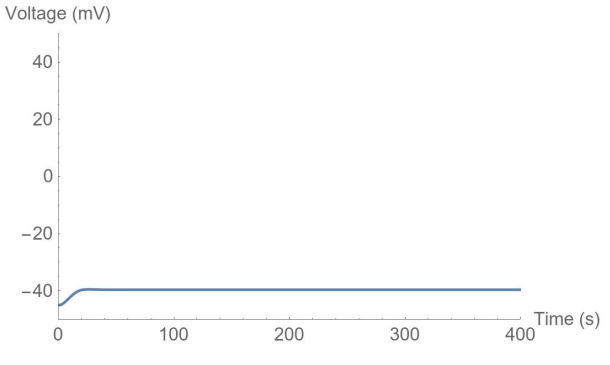

G

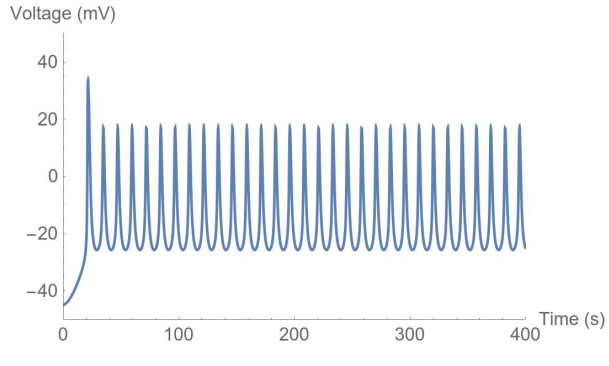

H

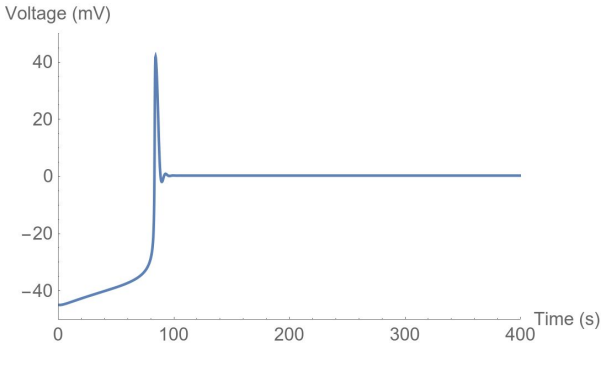

I

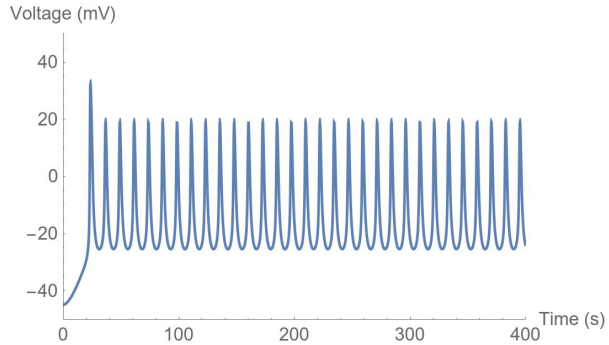

Figure 9, A-I: These full cell model results are discussed at length below. They were obtained by manipulating the Mathematica Manipulate object found in the attached notebook, FullCell.nb. Directions for how to obtain these using the manipulate are given by each header. If a value is not listed, assume it was set to zero as to remove the current from the model.

A: gdr = 3.5, gna = 4600, gl=0.1, cm=1.7

These settings are those which first gave us the sort of cyclic behavior we were expecting. Notably, the sodium and delayed rectifier dominate behavior - the other currents have minimal effect, as we see in B and C. This reveals that the delayed rectifier and sodium are doing their jobs, at least - when the sodium current depolarizes the cell, the delayed rectifier responds

with a heavy, delayed hyperpolarization. Note that the leak current is left in here - it's measurement is simplistic and its experimental value is trustworthy.

B: add gh=0.037, C: gh=0.37

The hyperpolarized-activated current should have a somewhat similar depolarizing effect to the sodium. In B and C, we see how the sodium term dominates at this value such that the hyperpolarized-activated current's only effect is shifting the curve to the left. However, further experimentation was unable to obtain repeated action potentials with lower sodium current values. This confirms the paper's assertion that the sodium current drives generation, and also confirms behavior of the hyper-polarized activated. The heightened value of 0.37 in figure C gives it a more pronounced effect, and brings it in line with experimental values of the delayed rectifier. This seems a more fitting ratio to us, but lacks biological evidence to back it up.
A note on C: the stunted spike at roughly 340 seconds is interesting, but is more likely an aberration of numerical integration than expected behavior. This seems to show the seams of our mathematical model.

D: add g0Ca=3.2, E: g0ca=16

The outward calcium-activated current seems to create space between the action potentials. This was confirmed in E, where increasing the value led to smaller, more spaced out spikes. At an arbitrarily larger value of 16, the g0ca dominates and causes the diminishing behavior seen in its current graph as well (figure 4A above). Note that the inward calcium current is acting at this time: the calcium buffer system in part causes this effect. The interplay between the currents at this point -- watching them trade off dominating terms and show their characteristics in relation to the others -- is quite interesting to our hypothesis. It seems that

certain combinations of currents will provide fruitful results to a limit. The ease with which they squash each other out confirms yet again the delicate sensitivity of the biological cell.

F: add gA=2.2, G: gA=0.22

Adding this current at it's default value crushes the other currents. Similarly to what we have done above, look at G for a more meaningful graph: here, the A-like seems to increase amplitudes slightly, and shift the curves slightly to the left, as seen at the cutoff at 400 seconds. The A-like has a smaller effect at this value, but the 2.2 value listed in the paper seems entirely off.

H: gd=0.34, g0ca=0.74, gA=0.38, others at initial values

These values were obtained from experimental evidence found in Table 1 of the first paper (Golowasch & Marder, 1992). Interestingly, the second paper (the one containing the model) used a delayed rectifier maximum conductance within a single standard deviation of that found experimentally, but uses quite different values for the calcium-activated and transient A-like currents. We can see a single spike, but the sodium seems to be too weak at this value to respond to the hyperpolarization driven by the delayed rectifier. However, upon scaling up the sodium current, the delayed rectifier proved too weak to generate action potentials. It seems reasonable to conclude that the authors altered these values in order to coax behavior out of the model.

I: gd=3.5, gna=4600, gh=0.37,g0ca=0.74,ga=0.38

This graph attempts to fix the delayed rectifier and sodium to where we previously saw action potential generation, while setting other currents to the experimentally found values. We get the desired result, with slightly more spaced spikes and a relatively large amplitude. We still

do not see the expected amplitude or period from the paper; attempts to obtain these all resulted in loss all resulted in one, but not the other.

Hypothesis

The clarity of the experimental data in the isolated currents allows a simple check for individual currents. Indeed, the simplistic i_{dr} and i_h are easily reproduced to match perfectly the paper's model and the approximately experimental data. The calcium is much more interesting; here it seems we are able to model the current rather well, but unable to model it's normalized conductance or steady states. This quirk demands further investigation.

Discussion

It perhaps makes the most sense to begin discussing our results in relation to the discrepancies with the paper's results. In biological data as well as the original results, tonic firing is expected at a baseline voltage of -45 to -50 mV -- that is, the model should give regular, unceasing action potentials without perturbations such as voltage clamp or current clamp conditions (Wang 2014). Also noted in the paper is that the sodium current should drive this behavior, while contributing mildly to the resting voltage of the cell. This informs a reading of the section describing the sodium current equations, which claims "the parameters were chosen to obtain firing of action potentials when the differential equations were integrated" in the full model cell (Buchholtz pg. 336). When the model is recreated entirely faithful to the values and equations as described in the paper, without the presence of any sort of perturbation, the

following graph is obtained:

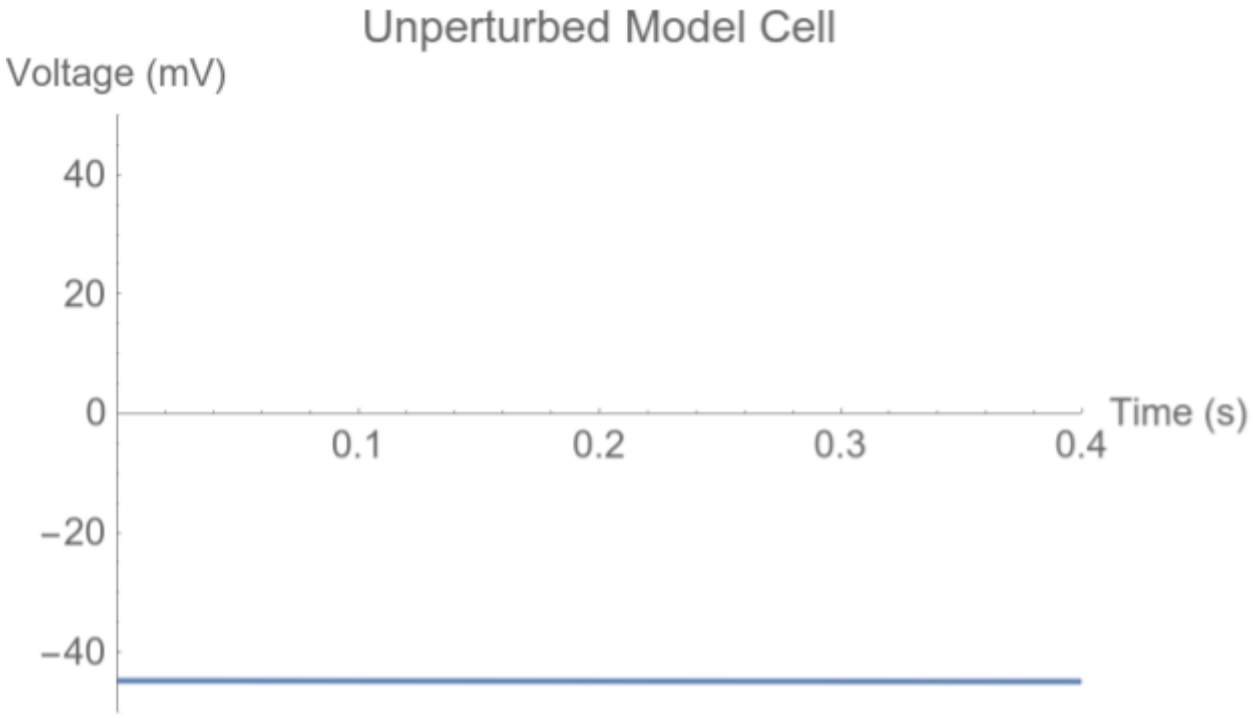

Figure 8. Behavior of the model cell when built in Mathematica using the paper's specifications.

This presents a problem. Issues in the original paper became apparent: it gives two relaxation parameters for the sodium current, for example, in line with other steady-state equations which lack a voltage-dependent relaxation and instead use a scalar value for relaxation. However, the sodium steady-state equations have Hodgkin-Huxley form voltage-dependent relaxation equations, and the reported parameters do not appear to be used anywhere. Indeed, their scalar values (10000 and 500 for activation and inactivation, respectively) are orders of magnitude different from those given by the stated equations, which range from zero to one. Using these values in lieu of the equations does not illuminate the model any further.

Another issue arises in the given membrane capacitance, 1.7 nF. The paper states this value was chosen in order to obtain accurate behavior from the model cell after construction.

Indeed, biologically observed values can differ depending on the measurement method, as Golowasch revisited in a 2009 paper (Golowasch 2009). My partner and I worked through the units on individual currents, however, and found that a value of 1700 gave accurate behavior of the individual currents -- otherwise, they vary significantly from what is expected.

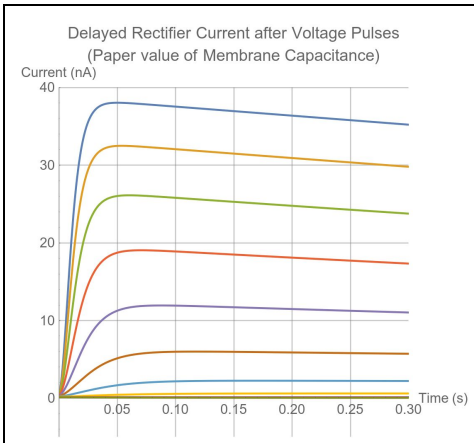

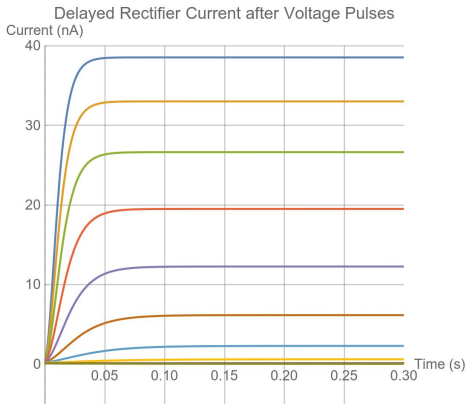

Figure 3A without *(left)* and with *(right)* the altered membrane capacitance.

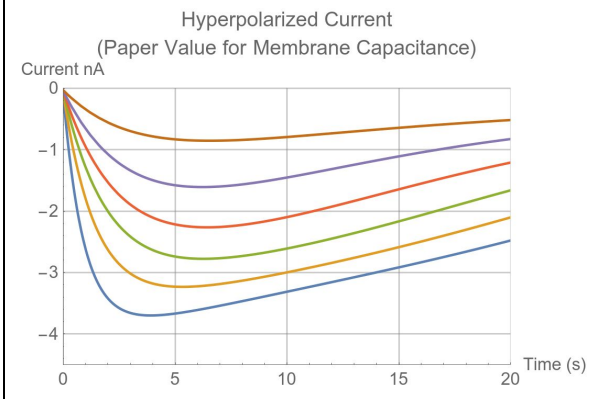

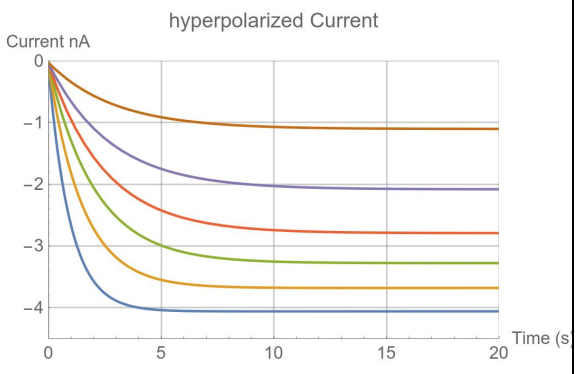

Figure 7A without *(left)* and with *(right)* the altered membrane capacitance.

I bring up these two errant details because they are stated in the paper to be critical to appropriate model performance, yet are presented in an unclear, conflicting fashion.

Original Hypothesis

The paper achieves its stated goal of creating and comparing model data to biological data in part by selectively altering parameter values for the sodium current (which generates

action potentials) and the membrane capacitance (which approximates the model to represent where in the cell biological measurements were taken) such that the model was useful to their purposes. My partner and I have found through our reconstruction that the model is incredibly sensitive to these parameters and their respective equations to the point that apparent errors in the paper render accurate reconstruction quite difficult.

This has a direct implication to our hypothesis. While troubleshooting the model, my partner and I created models with the currents most important to the creation of action potentials, the delayed rectifier, sodium, and leak currents. The sodium and rectifier currents swing back and forth in dominance between hyperpolarized and depolarized values, which is the fundamental relationship underlying the previously described tonic action potentials. Other currents play critical roles in the cell's response to voltage and current clamp scenario, but those identified above ought to satisfy our hypothesis that the cell could be broken down into components to better understand the behavior of the cell. However, the sensitive dependencies on particular values and the lack of biological reasoning for the selection of those values makes it quite difficult to attempt to understand the behavior of selected components of the model.

Extension Discussion

It is first worth noting that although our original hypothesis does not seem to be corroborated, we can make an adjacent statement through the extension. While our altered values lack biological significance, they do reveal the interactions between the effects of each current. As we adjust them piecemeal via the conductance value, we can see how some come to dominate other terms, others work in opposite directions to generate interesting behavior, and each acts as we might expect it to from individual analysis.

Interestingly, using experimental data found in the first paper as detailed above did not improve our results. They did help to explain some strange parameters: for example, the A-like current works within the cell using the experimental value, but dominates any sort of behavior at the listed conductance value. This anomaly has evaded our attempts at explanation, but the experimental value offers a compelling reason to dismiss it as a change made by the authors in order to produce their own results.

Similar Models and Future Work

The natural next step is to attempt to find our own parameter values that coerce accurate behavior from the model. Mathematica offers the Manipulate tool which allows us to directly search for these values. A reasonable (and likely) plan of action would be to first resolve our model incorporating the delayed rectifier, sodium, and leak currents by themselves. Good examples of neurons modeled in Mathematica can be found in chapter seven of Dr. Hillel Chiel's textbook, *Dynamics of Biological Systems*, (Chiel 2019) as well as directly from the Wolfram Foundation (Marom 2012) (Neske 2011).

That option of simplification exists, but over the years the scope of the field has increased, including in several directions indicated by the paper. A notable example is cable theory, which accounts for the fact that most neurons are not isopotential across their dendrites. An example of this produced by Golowasch in 2009 would be an excellent next step in the study of these systems, especially since it is a two-compartment model, a noted simplification in the paper (Golowasch 2009) (Buchholtz 1992 pg. 338).

Just as in class we examined growth of cells and growth of animal populations as two different, yet interrelated problems, the field of neuroscience is able to consider larger networks

of neurons in their own models. One sees exactly that in a 2018 paper, *Sloppy morphological tuning in identified neurons of the crustacean stomatogastric ganglion*. Here, the potential for variability between neural network constructs in different specimens and species is explored with an eye for cable theory and statistical testing. The thought of connecting these variations to a model cell is alluring, especially considering the finding that neuronal structures do not obey wiring optimization principles, instead being "governed by a space-filling mechanism that outweighs the cost of inefficient wiring" (Otopalik 2018).

A Note on the attached Mathematica Notebooks

Final model and figure recreations are all found in FullCell.nb. The other notebooks, specific to each current, were used to initially set up and test each current independently. They include loose thoughts and attempts at obtaining figures so that the process of discovery behind the recreation can be followed. They also include the initial condition calculations, which are left out of FullCell.nb to save space and keep the focus on the generation of results and discussion. I would suggest that readers begin by examining FullCell.nb, and then look at whatever current notebooks they would most like to examine in order to better understand our results and methods. In particular, the Transient A-like and Calcium System notebooks contain substantial notes and attempts at proper recreation. Be sure to quit the kernel prior to opening and observing each notebook; otherwise, functions and declarations will conflict and cause errors.

References

Buchholtz, F., Golowasch, J., Epstein, I. R., & Marder, E. (1992). Mathematical model of an identified stomatogastric ganglion neuron. *Journal of Neurophysiology, 67*(2), 332-340. doi:10.1152/jn.1992.67.2.332

Chizhov, A. V., & Amakhin, D. V. (2017). Method of experimental synaptic conductance estimation: Limitations of the basic approach and extension to voltage-dependent conductances. *Neurocomputing, 275*, 2414-2425. doi:10.1016/j.neucom.2017.11.017

Daur, N., Diehl, F., Mader, W., & Stein, W. (2012). The Stomatogastric Nervous System as a Model for Studying Sensorimotor Interactions in Real-Time Closed-Loop Conditions. *Frontiers in Computational Neuroscience, 6* (13). doi:10.3389/fncom.2012.00013

DeMaegd, M., Stein, W. (2018). Long-Distance Modulation of Sensory Encoding via Axonal Neuromodulation. 10.5772/intechopen.74647.

Fox, D. M., Tseng, H., Smolinski, T. G., Rotstein, H. G., & Nadim, F. (2017). Mechanisms of generation of membrane potential resonance in a neuron with multiple resonant ionic currents. *PLOS Computational Biology,13*(6). doi:10.1371/journal.pcbi.1005565

Golowasch, J., Gladis, T., Taylor, A., Patel, A., Pineda, A., Khalil, C., & Nadim, F. (2009). Membrane Capacitance Measurements Revisited: Dependence of Capacitance Value on Membrane Method in Nonisopotential Neurons. *Journal of Neurophysiology*, 102: 2161-2175. doi:10.1152/jn.00160.2009

Golowasch, J., & Marder, E. (1992). Ionic currents of the lateral pyloric neuron of the stomatogastric ganglion of the crab. *Journal of Neurophysiology, 67*(2), 318-331. doi:10.1152/jn.1992.67.2.318

Golowasch, J., Buchholtz, F., Epstein, I. R., & Marder, E. (1992). Contribution of individual ionic currents to activity of a model stomatogastric ganglion neuron. *Journal of Neurophysiology,67*(2), 341-349. doi:10.1152/jn.1992.67.2.341

Herrera-Valdez, M. A. (2012). Membranes with the Same Ion Channel Populations but Different Excitabilities. *PLoS ONE,7*(4). doi:10.1371/journal.pone.0034636

Chiel, H. (2019). 7. Modeling Excitability: Rhythmic Behavior and Bistability. *Dynamics of Biological Systems: A Quantitative Introduction to Biology*.

Neske, G. (2011). Neural Impulses: The Action Potential in Action. *Wolfram Demonstrations Project*. http://demonstrations.wolfram.com/NeuralImpulsesTheActionPotentialInAction/

Otopalik, A., Goeritz, M., Sutton, A., Brookings, T., Guerini, C., Marder, E. (2017). Sloppy morphological tuning in identified neurons of the crustacean stomatogastric ganglion. eLife 2017;6e22352. doi:10.7554/eLife.22352

Wang, L., Liang, P. J., Zhang, P. M., & Qiu, Y. H. (2014). Ionic mechanisms underlying tonic and phasic firing behaviors in retinal ganglion cells: a model study. Channels (Austin, Tex.), 8(4), 298–307. doi:10.4161/chan.28012